Engineering Structures 304 (2024) 117671

Contents lists available at ScienceDirect

Engineering Structures

journal homepage: www.elsevier.com/locate/engstruct

A collapse capacity prediction model based on ground motion duration

M. Liapopoulou [a,*], P.J. Stafford [a], A.Y. Elghazouli [a,b]

[a] Department of Civil and Environmental Engineering, Imperial College London, UK
[b] Department of Civil and Environmental Engineering, Hong Kong Polytechnic University, Hong Kong

ARTICLE INFO

Keywords:
Collapse capacity
Ground motion duration
Hysteretic behaviour
Incremental dynamic analysis

ABSTRACT

A prediction model for the seismic collapse capacity, which explicitly considers the influence of strong motion duration, in addition to key structural properties, is presented in this study. The model is developed based on incremental dynamic analyses of single-degree-of-freedom systems, employing a set of 67 earthquake records. The selected ground motions are matched by scaling to a target Eurocode 8 response spectrum, to avoid spectral shape bias in the results, and have varying 5–75% significant duration from about 5 s up to nearly 70 s. The structural models exhibit vibration periods in the range of 0.2 s to 3.0 s, varying negative slope in their post-capping branch from 0.02 to 0.30, and ductility between 1.0 and 6.0. Each oscillator is assigned bilinear and pinching hysteresis. Correlation coefficients are computed between the collapse capacity and the structural properties examined, as well as three ground motion parameters, which include the duration, Arias Intensity, and Husid plot slope. The period, post-capping slope, and ductility are all shown to be strongly correlated to collapse resistance while, among the ground motion variables, the duration exhibits the highest correlation. Based on iteratively reweighted least squares, predictive models are fitted to the collapse capacity data, providing estimates for the median collapse capacity and the variance. The predicted collapse capacity associated with the maximum duration considered is found to be up to 67% lower than that corresponding to the minimum duration. The rate of collapse capacity reduction with duration is shown to depend on the period, P-Δ level, hysteresis type, and the duration value itself. The proposed model is compared to those from previous studies and is shown to provide a simple and computationally efficient method to obtain collapse capacity estimates for specific target levels of strong motion duration.

1. Introduction

In the context of performance-based earthquake engineering, which is prevalent in current seismic design standards and regulations, one of the most crucial objectives is the avoidance of collapse. Eurocode 8 [1] defines the near-collapse limit state as the condition at which the structure is severely damaged but has not collapsed when subjected to rare seismic action with a return period of 2475 years, which corresponds to a 2% exceedance probability in 50 years. FEMA P-695 [2] postulates a methodology for evaluating the collapse capacity of structures based on incremental dynamic analyses (IDA) [3] and sets minimum requirements for the acceptable probability of collapse at the 2% in 50 years hazard level and the collapse margin ratio. Hence, accurate estimation of the seismic collapse potential is a key aspect in the design and assessment of new or existing structural systems. However, due to the large computational cost involved, research efforts have also aimed to develop simple, yet reliable, prediction models for the collapse capacity.

Most previous collapse capacity models focused on the influence of key structural properties. Such predictive relationships were developed based on analyses of either single-degree-of-freedom (SDOF) systems [4–7], which provided reliable estimates for first-mode-dominated structures and enabled a wider variation of the parameters of interest, or multi-degree-of-freedom (MDOF) systems [8,9]. In the case of SDOF oscillators, parameters such as the vibration period, slope of the negative stiffness branch of the pushover curve, ductility, strain hardening ratio, and type of hysteretic behaviour, were included in the predictive equations. On the other hand, studies adopting MDOF models employed parameters from static pushover analyses, as well as the fundamental period, number of stories, and yield base shear coefficient. In both cases, IDA [3] or similar incremental search techniques [10] were primarily employed for the collapse capacity estimation.

A common limitation in the above-noted models was the use of short-duration earthquake recordings and the disregard of duration effects.

* Corresponding author.
E-mail address: maria.liapopoulou17@imperial.ac.uk (M. Liapopoulou).

https://doi.org/10.1016/j.engstruct.2024.117671
Received 31 January 2023; Received in revised form 24 April 2023; Accepted 11 February 2024

The role of duration in collapse has been investigated by many researchers through comparing the collapse capacities of long and short ground motion sets. It is noteworthy that an unbiased comparison is only possible when other ground motion parameters which might affect the results are kept constant between the two record sets. Therefore, pairs of spectrally equivalent records were commonly employed to avoid spectral shape bias [11–13]. Other studies did not explicitly account for the differences between the long and short records response spectra but addressed the issue implicitly through the use of spectral displacement as the intensity measure (IM) [14,15]. Apart from the response spectrum, additional parameters related to the slope and shape of the Husid plot [16] or the incremental velocity [17] have been considered in isolating duration effects [18,19]. Notwithstanding the specific methodologies and assumptions, all these assessments led to the conclusion that longer ground motions reduce the collapse capacity compared to their short-duration counterparts.

The inclusion of duration in collapse prediction models, however, has only been addressed by relatively few investigations. An early study that offered equations for the collapse spectral ordinates incorporating duration was conducted by Bernal [20]. A suite of 24 records with 5–95% significant duration [21] ranging from about 2 s up to about 30 s was used in dynamic analyses of equivalent SDOF systems, which adequately captured the behaviour of MDOF frames. Various levels of period and stability coefficient were examined, as well as two types of hysteresis: elastoplastic and degrading. The proposed expressions for the elastoplastic systems incorporated not only the structural characteristics but also ground motion parameters, namely the peak ground velocity and displacement, and the 5–95% significant duration. However, the duration was not found to correlate significantly with the collapse capacity in degrading systems and was not included in the respective relationships, which contradicts recent studies that show a large influence of duration on the collapse of highly deteriorating structures [11,13]. A further limitation was the disregard of spectral shape effects in the development of the predictive equations.

Another collapse prediction model that incorporated the same duration metric was presented by Raghunandan and Liel [14]. This work addressed the issue of differences in response spectra among the records by using spectral displacement, S_d, which implicitly captures spectral shape effects, and proposed a predictive relationship for S_d at collapse, including the 5–95% significant duration as a predictor for both highly degrading and moderately degrading structures. Apart from duration, the fundamental period and a ductility flag were also employed in the prediction equation. The regression model was fitted to the results of IDAs on 17 reinforced concrete buildings subjected to 76 ground motion records with up to 271 s duration. The robustness of the model was demonstrated by cross-validation. However, the applicability of the model is limited by the lack of seismic hazard prediction equations in terms of S_d, as noted in the study.

More recently, Bravo-Haro et al. [22] and Liapopoulou et al. [19] developed predictive relationships for the collapse capacity of non-ductile and ductile SDOFs, respectively, incorporating instability and duration effects. The structural properties used as predictors in the proposed models were the period and level of P-Δ, determined by the stiffness of the negative branch in the pushover curve. In the case of ductile SDOFs, the ductility and strain hardening ratio were also included in the predictors. Both studies accounted for duration using spectrally equivalent records [13], which eliminated any spectral shape effects. Pairs of long and short records with equivalent response spectra were assembled, assuming that ground motions with 5–75% significant duration lower than 25 s for both horizontal components can be classified as short. Based on IDAs of the investigated structural configurations, distinct regression models were developed for each duration group. Although the suggested expressions provide a useful method to account for duration in collapse capacity estimation, the distinction between long and short ground motions was relatively vague, as an arbitrary limit was employed to indicate the transition from short to long records. Also, the definition of duration groups did not allow the consideration of specific duration values in collapse prediction.

The above discussion indicates that although the effect of duration on collapse is commonly acknowledged, it is still not adequately incorporated into collapse capacity predictions. Therefore, this study presents a novel collapse capacity model that explicitly account for the duration as a continuous variable, while also incorporating key structural properties. For this purpose, a suite of 67 ground motion records is assembled with uniformly distributed duration values in the range of about 5 s to 70 s. The selected recordings are scaled to match a target Eurocode 8 response spectrum, to ensure that the variation of collapse capacity is not caused by spectral shape differences among the records. IDAs are subsequently carried out on SDOF systems with bilinear or pinching hysteresis and varying period, P-Δ level, and ductility. Correlation analyses between the collapse capacity and a series of structural and ground motion parameters are carried out, to identify the most appropriate predictors of collapse. Regression models for the mean and variance of collapse capacity are then fitted to the IDA results. The proposed models are compared to those of previous studies in order to assess their efficiency and reliability.

2. Structural systems and record selection

2.1. Structural models

To simplify the structural behaviour and minimise the number of parameters under consideration, SDOF systems are employed in this work. While simple, these models have been widely used in the literature, as they can still provide significant insight into the behaviour of MDOF structures. The reduced computational time required for seismic analysis using SDOF models enables extensive parametric studies with large variations of basic properties to be carried out efficiently. For example, Adam and Jager (2012) [5] used SDOF models and derived collapse capacity spectra, based on short-duration records. Although such predictive relationships cannot be directly applied to real structures, they can be transformed into the MDOF domain through suitable equivalent SDOF models [23]. Hence, deriving equations for the collapse capacity of SDOF systems offers a very useful tool that provides fundamental insights into the influence of key parameters and gives a basis for predictions and underlying trends in real frames.

In this study, the SDOFs are modelled in OpenSees [24] using a rigid elastic beam-column element, with a mass m and a gravity load P assigned at the top node and a zero-length spring of initial elastic stiffness k located at the bottom node (Fig. 1a). Initial stiffness-proportional damping of $\xi = 5\%$ is assigned to the spring, and two types of hysteresis are considered: bilinear and pinching. The backbone curve consists of an initial elastic branch up to the yield point, followed by a plastic segment and then a hardening part with strain hardening ratio $\alpha = 3\%$. With the application of the gravity load P, the backbone curve is rotated by the stability coefficient θ due to the P-Δ effect, as shown in Fig. 1b. Various values are considered for the period T, the slope of the post-capping branch θ-α, and the ductility μ_c, according to Table 1, resulting in a

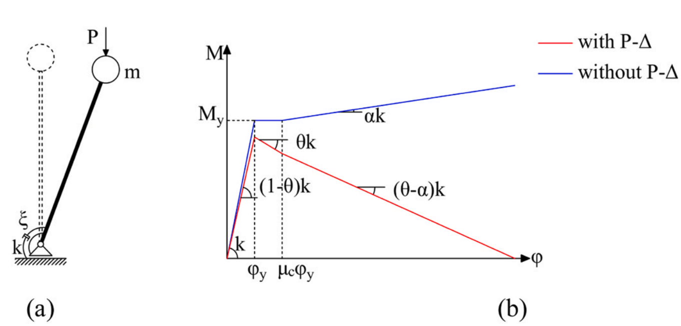

Fig. 1. (a) SDOF model and (b) moment-rotation curve.

Table 1
Parameters defining the structural models and corresponding values considered.

Parameter	Values considered
Period, T (s)	0.2, 0.5, 0.7, 1.0, 2.0, 3.0
Negative stiffness, θ-α	0.02, 0.04, 0.06, 0.10, 0.20, 0.30
Ductility, μ_c	1.0, 2.0, 4.0, 6.0

total of 144 combinations. The mass m and load P of each SDOF are computed based on its period and post-capping slope, respectively.

It should be noted that the model defined herein is not linked to a specific structure in the context of this study but can represent any structural system within the range of parameters considered and with a hysteretic response that can be adequately described by the bilinear or pinching hysteresis assigned to the model. The period, P-Δ level, and ductility, are varied within typical limits of structures. A significant limitation, however, is the inability to capture the contribution of higher modes. This implies that high-rise buildings, such as a 20-story steel frame, cannot be effectively represented through this simple model. Therefore, the model is not suitable to describe the response of structures that are significantly affected by higher-mode effects. Regarding the material type, the bilinear hysteresis is characteristic of many steel structures, while the pinching model may represent various concrete buildings. However, the response of other structural systems may not be captured directly through the SDOF model of this study.

2.2. Ground motion records

An initial catalog of records is extracted from the NGA-West-2 [25], the K-Net [26] and kik-net databases [27], considering exclusively non-pulse-like records from strong earthquakes (M>6.0) and with relatively large PGA values (PGA>0.1 g) to avoid excessive scaling at collapse level. The Shahi and Baker [28] algorithm is employed for the pulse classification, which uses wavelet transform in the two orthogonal components to identify pulses and characterises them based on a support vector classification boundary. Pulse-like records are excluded from this research due to their special features that require additional parameters to be considered. Based on these criteria, a total of 12,196 recordings are assembled, which cover a wide range of duration. It should be noted that records from the K-Net and kik-net databases were initially retrieved as raw data and were then processed as described in Appendix A.

Since the aim is to develop a model for the collapse capacity that includes duration effects, the response spectra of the selected records must be kept constant, to ensure that the differences in response are primarily due to duration and not due to spectral shape bias. The Eurocode 8 Type 1 elastic response spectrum for Ground Type B, Importance Class II and a reference peak ground acceleration of 0.36 g, is chosen as the target spectrum. The use of Type 1 spectrum is justified by the large magnitude earthquakes considered in this study. The Ground Type B corresponds to shear-wave velocity $V_{s,30}$ between 360 and 800 m/s, which is consistent with most of the ground motion records herein, and the Importance Class II refers to ordinary buildings. The reference peak ground acceleration is selected based on the highest seismic zone in Greece, according to the National Annex to Eurocode 8 [29].

Spectral matching is performed by scaling each record, such that the sum of squared errors SSE between the logarithmic spectral ordinates of the scaled record and the target spectrum is minimised. The SSE is computed based on 200 periods logarithmically equally spaced from 0.04 s to 6.0 s, according to Eq. 1, and the required scale factor SF is estimated as the ratio of the geometric mean of the target spectral ordinates to the geometric mean of the spectral ordinates of the record, based on Eq. 2. Records that required a scale factor larger than 6 are discarded to prevent large initial scaling. The limit of 6 for the scale factor is marginally higher than typical limits used in previous studies [11,13] but is still within the range that allows legitimate scaling. It was selected such that an adequate number of records with a close match to the target spectrum is available. It is noteworthy that the periods considered herein correspond to a range of 0.2 T_{min} to 2 T_{max}, based on the minimum and maximum period of the SDOFs, which is consistent with the recommendations of Eurocode 8 [29].

$$SSE = \sum_{i=1}^{200} \left[\ln S_a{}'(T_i) - \ln(SF \bullet S_a(T_i))\right]^2 \tag{1}$$

$$SF = \frac{\sqrt[200]{\prod_{i=1}^{200} S_a{}'(T_i)}}{\sqrt[200]{\prod_{i=1}^{200} S_a(T_i)}} \leq 6 \tag{2}$$

The 5–75% significant duration [30], denoted herein as Ds, is employed to measure the strong motion duration. This metric has been extensively used in investigations of duration effects on collapse and was identified as the most suitable for this purpose in previous studies [13, 31]. To ensure that a wide range of duration values is covered, 67 records with the best possible spectral match and relatively uniformly distributed duration up to nearly 70 s are selected. Attention is paid to avoid the inclusion of both horizontal components of the same recording. The number of records from the same earthquake cannot be further diminished as, at the longer duration range (Ds>40 s), many of the compatible ground motions to the Eurocode 8 spectrum are from the 2011 Tohoku earthquake. The 5% acceleration response spectra of the individual records, along with the target spectrum, are plotted in Fig. 2. Characteristics of the selected ground motions, including the number of records from each earthquake, the magnitude, and range of duration, are given in Table 2.

3. Numerical assessments

The collapse capacities of the examined SDOF systems subjected to the selected ground motion records are estimated based on IDA [3]. The IM employed in the analyses is the spectral acceleration at the fundamental period $S_a(T)$ divided by the gravitational acceleration g and the base shear coefficient γ. The ductility μ, defined as the ratio of the displacement at the tip of the SDOF divided by the yield displacement, is adopted as the engineering demand parameter (EDP). The collapse limit state is defined either based on the last point of numerical convergence or the last point where the ductility is lower than the maximum ductility from static pushover analysis. The latter is chosen as the threshold for collapse due to the connection between the static pushover and incremental dynamic analysis [32]. The collapse capacity CC is defined as the

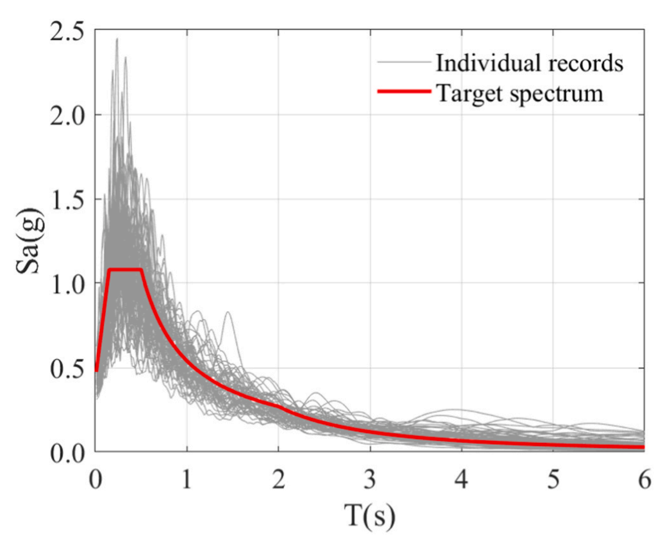

Fig. 2. Acceleration response spectra of the selected records and target response spectrum.

Table 2
Characteristics of selected ground motions.

Earthquake	M	Number of records	Ds range (s)
1999 Chi-Chi, Taiwan	7.62	7	16.24-35.50
1999 Chi-Chi, Taiwan-03	6.20	1	10.35
1999 Chi-Chi, Taiwan-04	6.20	1	6.75
1999 Chi-Chi, Taiwan-05	6.20	1	7.71
1994 Northridge-01	6.69	5	6.78-12.67
1999 Hector Mine	7.13	1	13.14
1990 Manjil, Iran	7.37	1	16.41
1952 Kern County	7.36	1	10.19
1992 Landers	7.28	5	20.90-30.48
2012 Kamaishi	7.30	5	35.64-39.69
2005 Northwest of Chiba	6.00	1	21.09
2003 Hokkaido	8.30	4	14.01-24.71
2004 Hokkaido	7.00	1	7.96
2005 Hokkaido	6.30	1	5.84
2011 Miyagi	7.10	2	20.49-21.61
2011 Tohoku	9.00	30	40.45-69.24

spectral acceleration at the state of collapse $S_{ac}(T)$, divided by the gravitational acceleration g and the base shear coefficient γ, according to Eq. (3) [5] as follows:

$$CC = \frac{S_{ac}(T)}{g\gamma} \tag{3}$$

3.1. Influence of ground motion parameters

In this section, the main ground motion parameters are investigated to identify those that are highly correlated with the collapse capacity and are therefore the most appropriate to include in the prediction model. As noted above in Section 2.2, the 5–75% significant duration is adopted to represent the strong motion duration. The influence of Husid plot [16] is represented by the total Arias Intensity IA_{tot} [33], which quantifies the energy input of the record, and the slope, m, of the Husid plot, defined as the ratio of the 5–75% Arias Intensity to the 5–75% significant duration. This metric indicates the rate of seismic energy arrival and was recently used as an additional parameter to isolate the effects of duration between long and short spectrally equivalent records [18].

Fig. 3 shows scatter plots and trend lines of the logarithmic collapse capacity, with the logarithm of each examined ground motion parameter for a specific SDOF system (T = 2.0 s, θ-α = 0.04, μ_c=1.0 and bilinear hysteresis). The Pearson correlation coefficients r and the p-values associated with these correlation coefficients are reported in each figure panel. A decreasing tendency is discerned between the logarithm of collapse capacity and the logarithm of duration, as well as the logarithm of total Arias Intensity. It is evident that longer records or those with greater energy input tend to reduce the structural collapse resistance. The Husid plot slope, on the other hand, appears to be beneficial to collapse, as shorter records are usually associated with larger slopes. Among the three ground motion parameters, the highest levels of correlation are observed with respect to duration (|r|=0.51), while the metrics related to the Husid plot exhibit relatively low correlation with structural collapse. The p-values corresponding to correlations with the duration and the total Arias Intensity are lower than the significance level of 0.05, thereby indicating statistical significance. On the other hand, the Husid plot slope does not exhibit statistically significant correlation with the capacity.

To examine the influence of the hysteresis type and the system stiffness, two variants of the previously considered system are assessed, namely a pinching SDOF with T = 2.0 s, θ-α = 0.04, and μ_c= 1.0, and a bilinear SDOF with T = 0.5 s, θ-α = 0.04, and μ_c= 1.0. The correlation

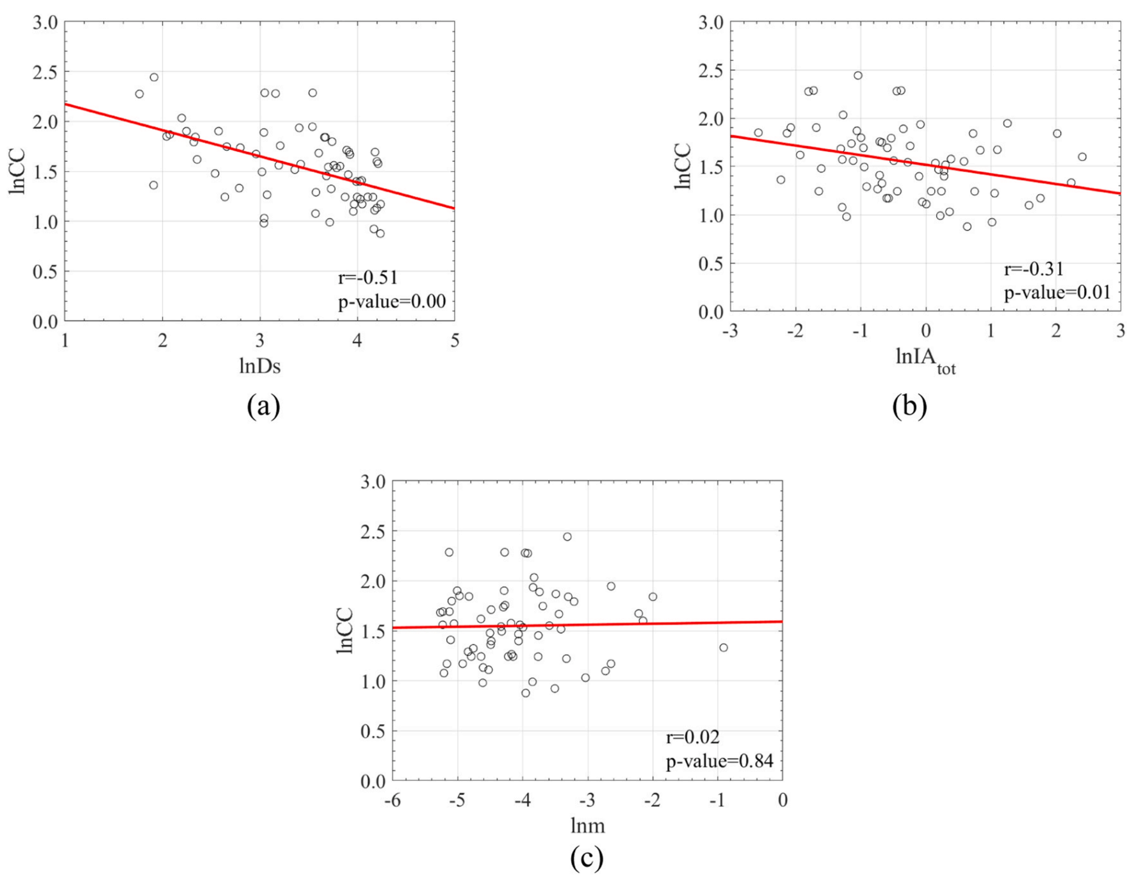

Fig. 3. Correlation between logarithmic collapse capacity and logarithmic ground motion parameters for a system with T = 2.0 s, θ-α = 0.04, μ_c= 1.0, and bilinear hysteresis. The ground motion parameters are: (a) 5–75% significant duration, (b) total Arias Intensity, and (c) slope of Husid plot.

coefficients and associated p-values of these SDOFs are given in Table 3 and may be directly compared to the values corresponding to the initial SDOF from Fig. 3. The pinching system is shown to exhibit a lower degree of correlation with duration, while the total Arias Intensity and the slope of the Husid plot are not statistically significantly correlated with the collapse in this case. The more rigid system, on the other hand, shows a stronger correlation with the duration and a weaker correlation with the total Arias Intensity. As observed for the initial SDOF, the correlation between the Husid plot slope and the collapse capacity is not statistically significant.

Boxplots of the absolute correlation coefficients between the logarithmic collapse capacity and the logarithm of duration and total Arias Intensity are given in Fig. 4. Only statistically significant results are considered (p-value<0.05). Absolute values of the correlation coefficient are used, as the strength rather than the direction of the association is relevant herein. Similar to the observations made for the specific SDOF in Fig. 3, the 5–75% significant duration exhibits the greatest correlation with collapse, with a median correlation coefficient of 0.53 and 0.35 for bilinear and pinching hysteresis, respectively. On the other hand, the total Arias Intensity is correlated to a lesser extent with collapse, displaying median correlation coefficients of about 0.35 to 0.27. The dispersion of these correlation coefficients among the various SDOFs is also much lower, compared to the significant duration. In fact, the number of systems that yielded statistically significant results for IA_{tot} is relatively small. It is noteworthy that the minimum degree of correlation is nearly the same for both examined parameters and types of hysteresis. These minimum values correspond to short periods and/or large P-Δ levels, which result in low collapse resistance, irrespectively of the specific ground motion characteristics. Based on these observations, it can be concluded that the 5–75% significant duration is the most influential ground motion parameter in terms of its association with structural collapse and can therefore be deemed a predictor of collapse capacity.

3.2. Influence of structural properties

The effect of the structural properties considered in this paper (period, level of P-Δ, and ductility) on the collapse capacity is evaluated herein. Accordingly, the Pearson correlation coefficients between the logarithmic collapse capacity and each structural parameter are computed. Due to the lower number of data points compared to the scatterplots with ground motion parameters, large absolute values of correlation coefficients are expected. This, however, does not imply that the structural properties are associated to a larger degree with collapse. In fact, to demonstrate their significance, the least-squares linear trend slopes are also noted below.

Representative scatterplots are shown in Fig. 5 for the case of a 2011 Tohoku earthquake recording and considering the following structural properties: T = 2.0 s, θ-α = 0.06, μ_c= 1.0, and bilinear hysteresis. As expected, all three parameters are strongly correlated with seismic collapse; however, such large |r| values should be interpreted with caution due to the small sample size in each figure panel. The slopes of best-fit lines can provide useful insight into the importance of each variable to structural collapse. Relatively large changes in lnCC are noted with changes in period and P-Δ level, while lnCC exhibits a slightly decreasing trend with the ductility, as indicated by the relevant slope values. The reason that the ductility has a negative impact on the collapse resistance in this study is due to the negative slope in the backbone curve intermediate branch, as also noted in [19].

To provide insight into the duration effect, the correlation coefficients and associated p-values for the same SDOF system (T = 2.0 s, θ-α = 0.06, μ_c=1.0, and bilinear hysteresis) subjected to a short-duration record from the 2004 Hokkaido earthquake (Ds=7.96 s) are given in Table 4. By comparing these values with those corresponding to the 2011 Tohoku long duration record from Fig. 5, it is observed that the degree of correlation between the collapse capacity and structural properties is nearly unaffected by the strong motion duration. As noted before, these large |r| values are associated with the small sample size, and hence, the duration of the considered earthquake record is not a significant factor.

Boxplots of the absolute correlation coefficients and slope values, considering all cases with p-values lower than 0.05, are shown in Fig. 6, for bilinear hysteresis. In Fig. 6b, the slope values corresponding to T and μ_c are measured on the left-hand axis, while those corresponding to θ-α are measured on the right-hand axis. As noted before, all examined structural parameters are strongly correlated with the collapse capacity; the correlation coefficients with period and P-Δ vary between about 0.8 and 1.0, exhibiting a median value close to 0.9. With respect to ductility, the range of correlation narrows down to 0.95–1.0, which indicates that the collapse capacity varies virtually linearly with it. The median absolute slopes of the linear regression lines with period is about 0.3, and about an order of magnitude higher when the P-Δ level is considered as the independent parameter. These values imply relatively large changes in lnCC with period and P-Δ. On the contrary, the median |s| is nearly 0.1 for the ductility, thereby suggesting limited influence on the collapse resistance. Similar observations can be made for pinching hysteresis. Accordingly, the period and P-Δ level can be considered as the most important parameters, while inclusion of the ductility in the collapse capacity prediction model may be less critical.

Table 3
Correlation coefficients and p-values between logarithmic collapse capacity and logarithmic ground motion parameters for a pinching system (with T = 2.0 s, θ-α = 0.04, μ_c=1.0) and a rigid system (with T = 0.5 s, θ-α = 0.04, μ_c=1.0, and bilinear hysteresis).

	Pinching system			Rigid system		
	lnDs	$\ln IA_{tot}$	lnm	lnDs	$\ln IA_{tot}$	lnm
r	-0.32	-0.12	0.10	-0.58	-0.25	0.14
p-value	0.01	0.34	0.41	0.00	0.04	0.25

4. Prediction models

4.1. Regression analyses

Given the relatively large number of predictors and the nonlinearity of the response, the definition of a suitable functional form for the regression model is not straightforward. To facilitate this process, a simple linear regression (Eq. (4)) is initially performed between the logarithmic collapse capacity and the logarithmic duration for each SDOF, taking advantage of their relatively strong correlation.

$$\ln CC = m + n \bullet \ln Ds \tag{4}$$

The estimated coefficients m and n are then regressed on the structural properties T, θ-α, and μ_c, considering the data of all 144 SDOFs for each hysteresis type. After testing many combinations of the predictor variables, Eqs. (5) and (6) are selected as those with the closest fit to the data.

$$m = m_1 \ln T + m_2 (\theta - \alpha)^{m_3 \ln T + m_4} + m_5 \mu_c \tag{5}$$

$$n = n_1 \ln T + n_2 (\theta - \alpha)^{n_3} \tag{6}$$

The coefficients m and n estimated from the linear regression between lnCC and lnDs (Eq. (4)), along with their predicted counterparts from Eqs. (5) and (6), are plotted for all combinations of T and θ-α, and a fixed level of ductility (μ_c=1.0) in Fig. 7, for bilinear systems. The corresponding plot for pinching systems is given in the Appendix. Eq. (5) yields m values very close to the target points, which virtually coincide with the surface, while Eq. (6) also has a high level of accuracy, except for some combinations of period and P-Δ, where larger deviations are notable. The ductility is not included in Eq. (6), as this did not result in

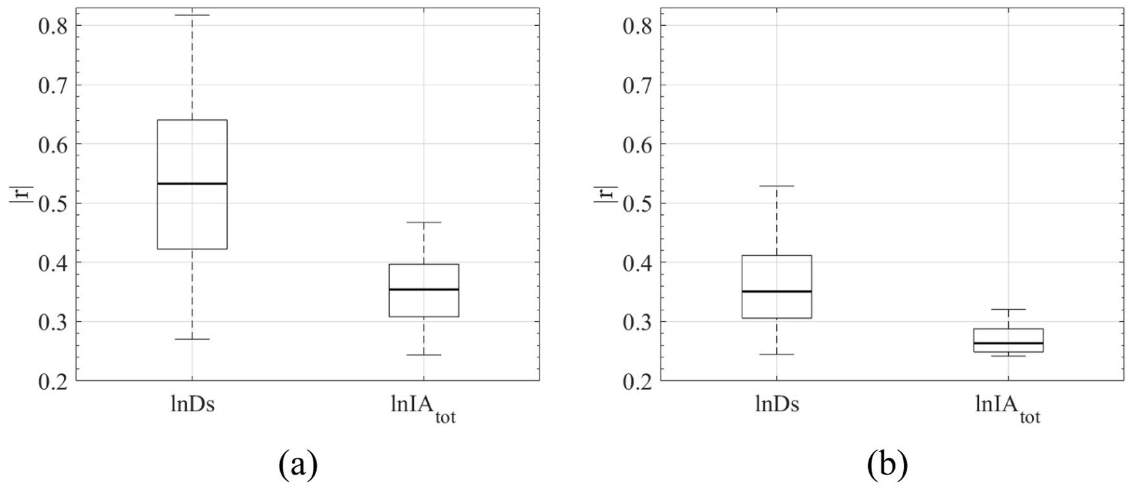

Fig. 4. Boxplots of absolute correlation coefficient between logarithmic collapse capacity and logarithmic ground motion parameters for: (a) bilinear hysteresis, and (b) pinching hysteresis.

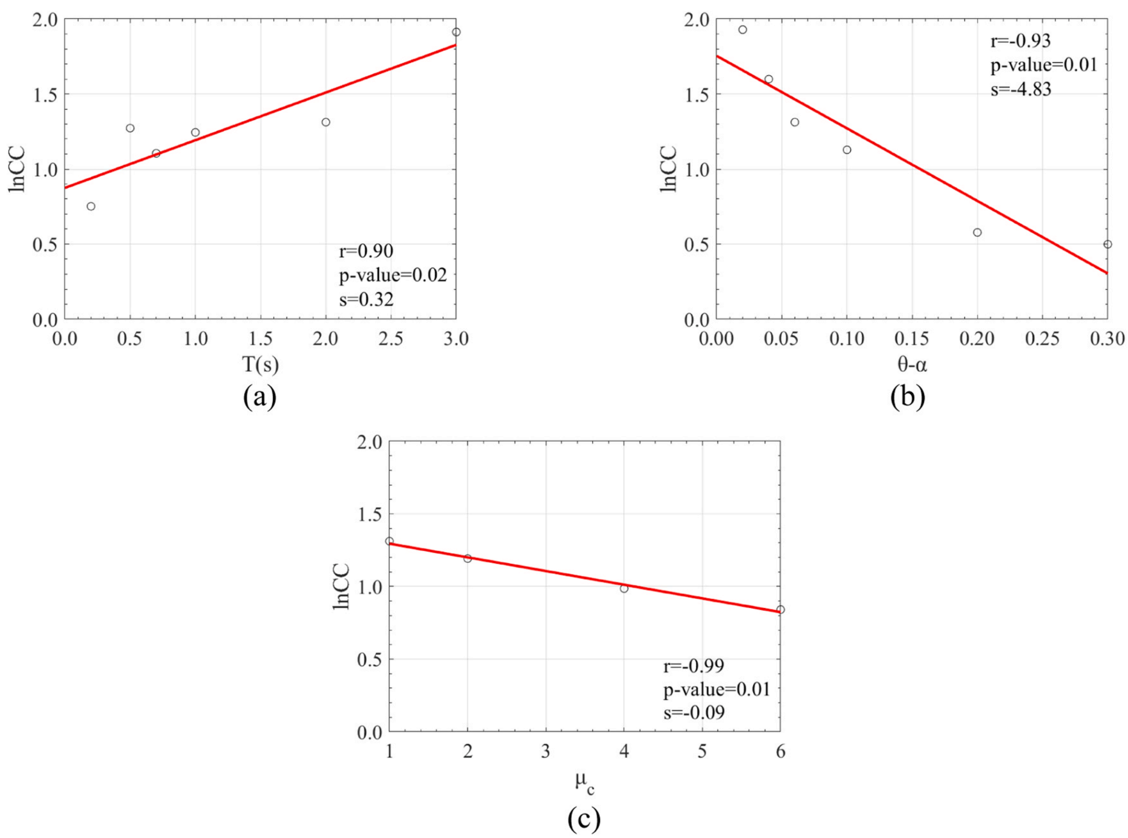

Fig. 5. Correlation between logarithmic collapse capacity and structural parameters for a system with T = 2.0 s, θ-α = 0.06, μ_c= 1.0, and bilinear hysteresis, subjected to the 2011 Tohoku earthquake. The structural parameters are: (a) period, (b) level of P-Δ, and (c) ductility.

Table 4
Correlation coefficients and p-values between logarithmic collapse capacity and structural parameters for a system with T = 2.0 s, θ-α = 0.06, μ_c= 1.0, and bilinear hysteresis, subjected to the 2004 Hokkaido earthquake.

	T	θ-α	μ_c
r	0.90	-0.83	0.99
p-value	0.01	0.04	0.01

considerable improvement of the predictions. This denotes that the effect of duration on SDOFs is primarily dependent on the period and P-Δ level, which is consistent with findings in previous studies [19].

Combining Eqs. (5) and (6) with Eq. (4), Eq. (7) is derived and employed in the predictive model. The variance is modelled as a quadratic function of the logarithmic duration (Eq. (8)), which is chosen after comparing different functional forms. It is noteworthy that only duration is considered in the variance model, as including the rest of the independent variables did not result in significant improvement of accuracy.

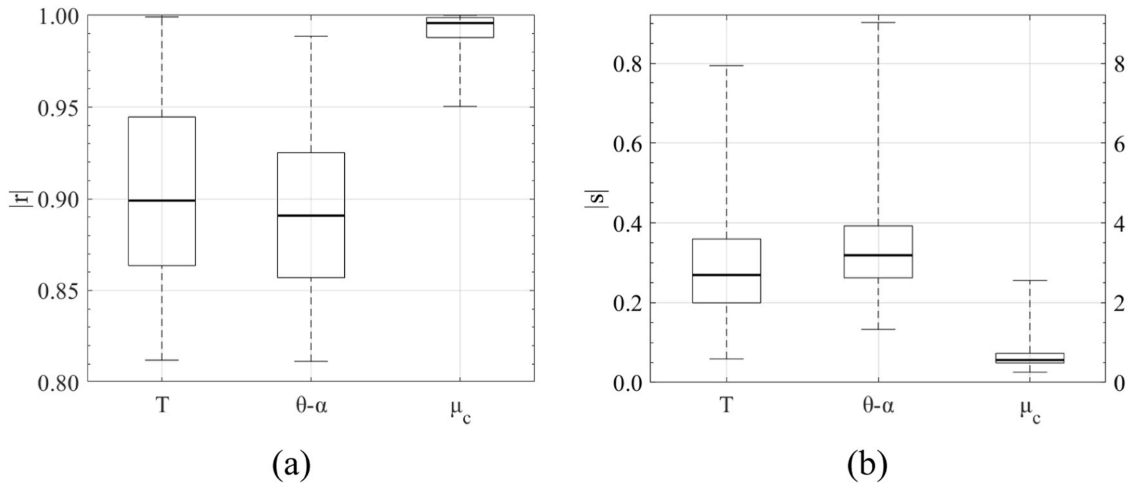

Fig. 6. Boxplots of (a) absolute correlation coefficient and (b) absolute slope between logarithmic collapse capacity and structural parameters for bilinear hysteresis.

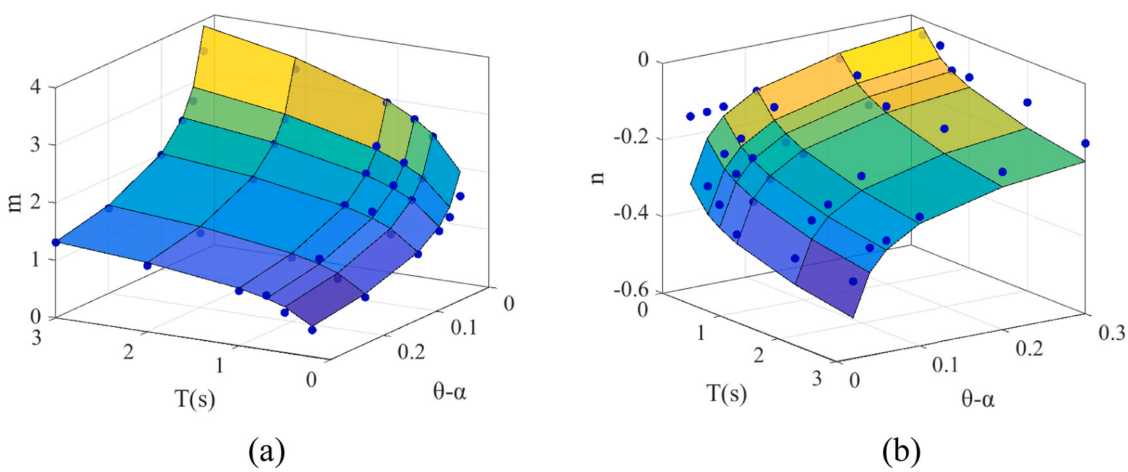

Fig. 7. Predicted (surface plot) and target (spheres) coefficients m and n for bilinear systems with μ_c= 1.0.

$$\ln CC = k_1 \ln T + k_2(\theta - \alpha)^{k_3 \ln T + k_4} + k_5\mu_c + [k_6 \ln T + k_7(\theta - \alpha)^{k_8}]\ln Ds \quad (7)$$

$$\sigma^2_{\ln CC} = p_1 + p_2 \ln Ds + p_3 \ln Ds^2 \quad (8)$$

The coefficients k_1 to k_8 and p_1 to p_3 are estimated based on iteratively reweighted least squares (IRLS) regression. Firstly, an ordinary least squares (OLS) regression is carried out and initial values of the regression coefficients k_1 to k_8 are estimated. Next, the squared residuals are computed and fitted to the variance model, thus providing an initial estimate of the coefficients p_1 to p_3. Based on the variance model, the weights are derived as the reciprocal of the variance ($w = 1/\sigma^2_{\ln CC}$). Weighted least squares (WLS) regression is then carried out to refit the data to the mean model. The procedure is repeated until the weights computed from two consecutive iterations are practically identical. The coefficients obtained through this process are given in Table 5 for bilinear and pinching hysteresis.

The predictive ability of the proposed regression models was tested through cross-validation. More specifically, the dataset was randomly partitioned into a testing set containing 20% of the data and a training set that comprises the rest of the data. This random split of the data was repeated 1000 times. For each split, the regression models were refitted to the training set and validated using the testing set. The mean square prediction error of the i^{th} repetition $MSPE_i$ was calculated as the sum of squared differences between the testing data $\ln CC_{test,i}$ and the predicted data $\ln CC_{pred,i}$, based on the refitted regression model, divided by the testing sample size n, as shown in Eq. (9). The mean square prediction error of the model was then evaluated as the mean error over all repetitions, according to Eq. (10).

$$MSPE_i = \frac{1}{n}\sum_{j=1}^{n}\left(\ln CC_{test,i,j} - \ln CC_{pred,i,j}\right)^2 \quad (9)$$

$$MSPE = \frac{1}{1000}\sum_{i=1}^{1000} MSPE_i \quad (10)$$

The resulting mean regression lines from each repetition, as well as the mean regression lines from the full dataset, are plotted in Fig. 8 for a bilinear and a pinching system with T = 3.0 s, θ-α = 0.02, and μ_c= 1.0.

Table 5
Regression coefficients for bilinear and pinching hysteresis.

	k_1	k_2	k_3	k_4	k_5	k_6	k_7	k_8	p_1	p_2	p_3
Bilinear	0.339	0.686	-0.015	-0.381	-0.063	-0.061	-0.072	-0.426	0.230	-0.088	0.011
Pinching	0.299	0.635	-0.023	-0.363	-0.022	-0.038	-0.035	-0.461	-0.169	0.155	-0.024

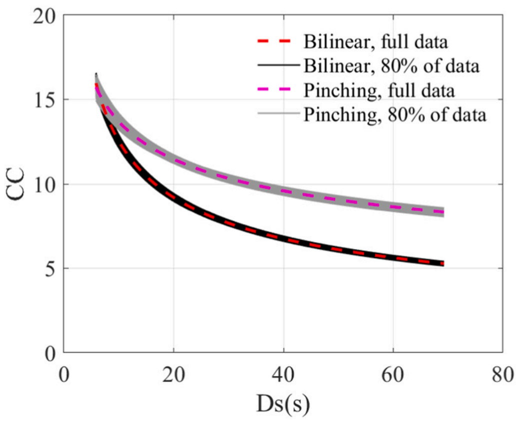

Fig. 8. Predicted collapse capacity against duration for T = 3.0 s, θ-α = 0.02, μ_c= 1.0 and both types of hysteresis. Models fitted to the full dataset (dashed lines) and to training sets that include a random 80% of the data (solid lines) are presented.

The models fitted to the smaller training sets deviate around the full model lines, creating a shaded area. For both types of hysteretic behaviour, the spread around the mean lines is relatively limited and the models based on the training sets are still close to the mean lines. Although not shown here for brevity, this holds true for all combinations of structural parameters. Hence, the bilinear and pinching models do not depend strongly upon the specific dataset used to fit them.

The mean squared prediction error, along with the mean square error of the full models, are given in Table 6. It is observed that the prediction error is only slightly larger than the corresponding standard error of the regression for both hysteresis types, which indicates the strong predictive ability of the models on new statistical samples.

The proposed regression models also satisfy the assumption of homoscedasticity, which can be confirmed by a visual inspection of the standardised residuals. Relevant plots of the residuals against the fitted values are included in Appendix B.

Finally, it should be noted that the collapse capacity model presented herein is not directly applicable in a quantitative sense to any type of structure, due to the limitations of the SDOF model based on which it was derived, as explained in Section 2.1. However, it provides a fundamental assessment and understanding of the role of duration in simple systems and can, with appropriate validation, be extended to specific MDOF structures.

4.2. Collapse capacity models

The regression models developed in the previous section are applied herein followed by a discussion on the role of duration. Adopting the assumption that the collapse capacity is lognormally distributed, which has been commonly used in previous studies [34], the median (50%), 16%, and 84% predicted collapse capacities can be obtained from the regression model. These are plotted in Fig. 9 against duration for bilinear and pinching systems with fixed period, P-Δ level, and ductility (T = 3.0 s, θ-α = 0.02, μ_c=1.0). The capacity values derived from IDAs are also shown with circles in the same figure. For both types of hysteretic behaviour, increased duration leads to reduced collapse resistance. The rate of reduction is larger at short duration levels and reduces as the duration increases. For example, the median collapse capacity predicted for the bilinear system reduces by about 46% when subjected to a significant duration of 40 s compared to a 10 s duration, while an increase in duration from 40 s to 70 s results in only 21% further reduction in capacity. This implies that the duration effect saturates at relatively long events, as the system limits are reached.

Table 6
Mean square error and mean square predicted errror for bilinear and pinching models.

	MSE	MSPE
Bilinear	0.0624	0.0625
Pinching	0.0730	0.0732

In Figs. 10 and 11, the median predicted collapse capacity of bilinear and pinching systems is plotted against duration for varying levels of period and P-Δ, respectively, while keeping all other parameters constant. A common trend in all cases, is the reduced collapse resistance of systems subjected to longer duration earthquakes. The amount and rate of this decrease, however, depends on the specific properties of the SDOF. Higher reduction rates and larger capacity losses are obtained at longer periods and lower P-Δ levels. In contrast, at very low period or high θ-α values, an increase in duration above about 40 s does not result in any notable reduction in collapse resistance. The reason for the limited influence of duration on these systems can be explained by considering that short periods and large θ-α values correspond to rigid structures and those with very steep slope on the decreasing branch of the pushover curve, respectively. In both cases, these systems tend to collapse relatively early; thus, longer duration earthquakes cause hardly any difference in the response. It is also noted that bilinear systems exhibit larger collapse reduction rates than their pinching counterparts. This can be attributed to the longer 'inner' loops in the force-displacement response of the latter, which renders them less prone to duration effects, as explained in [19].

To better understand the effects of duration, the maximum percentage reduction in median collapse capacity is quantified based on the minimum and maximum duration of the records employed herein, namely 5.84 s and 69.24 s. The results are plotted for varying period and P-Δ level in Fig. 12, considering both types of hysteretic behaviour. As expected, longer periods and lower P-Δ effects both lead to larger collapse capacity reductions. The capacity of bilinear systems is affected to a greater extent by strong motion duration, compared to their pinching counterparts. Up to about 67% of reduction is estimated for bilinear and around 47% for pinching hysteresis, which correspond to a 3.0 s period and a P-Δ level of 0.02. Hence, an underestimation of the expected strong motion duration could result in significant overestimations of the collapse resistance. This emphasises the need to incorporate duration in collapse assessment procedures, particularly in regions where long records contribute to the seismic hazard, as otherwise unconservative estimates would be obtained.

4.3. Collapse fragility curves

Collapse fragility curves are cumulative distribution functions of the collapse capacity and represent an essential part of seismic hazard estimation. Assuming that collapse capacity is lognormally distributed, the fragility curve can be estimated based on Eq. (11), as follows:

$$F_X(\mathrm{x}) = \Phi\left(\frac{lnx - \mu_{\ln CC}}{\sigma_{\ln CC}}\right) \tag{11}$$

where lnx is the specific value of lnCC at which the fragility curve F_x is evaluated, and Φ is the cumulative distribution function of the standard normal distribution.

Fig. 13 illustrates collapse fragility curves of a bilinear and pinching system for varying duration from 10 s to 70 s with 20 s increments. A period of 3.0 s, P-Δ level of 0.04, and ductility of 6.0 are considered. As the duration increases, lower median collapse capacities and lower dispersions are observed, indicating increased vulnerability to longer ground motions. For the same ground motion duration, the pinching model exhibits larger median collapse capacity and dispersion than its bilinear counterpart. The superior performance of pinching systems, which is associated with their longer 'inner loops' in the force-displacement response, is consistent with results of previous studies

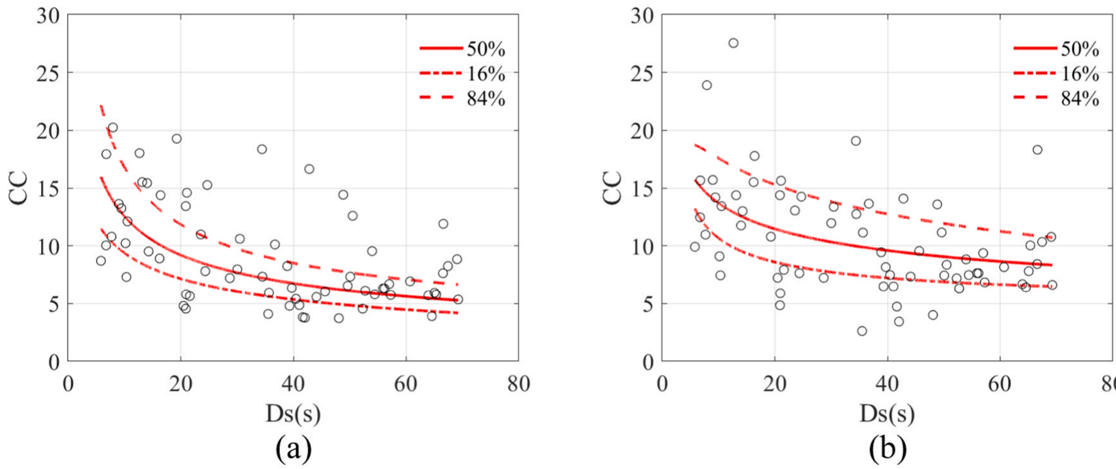

Fig. 9. 50%, 16%, and 84% predicted collapse capacity against duration for systems with T = 3.0 s, θ-α = 0.02, μ_c= 1.0 for: (a) bilinear hysteresis, and (b) pinching hysteresis. The collapse capacity results from IDAs are also shown with circles.

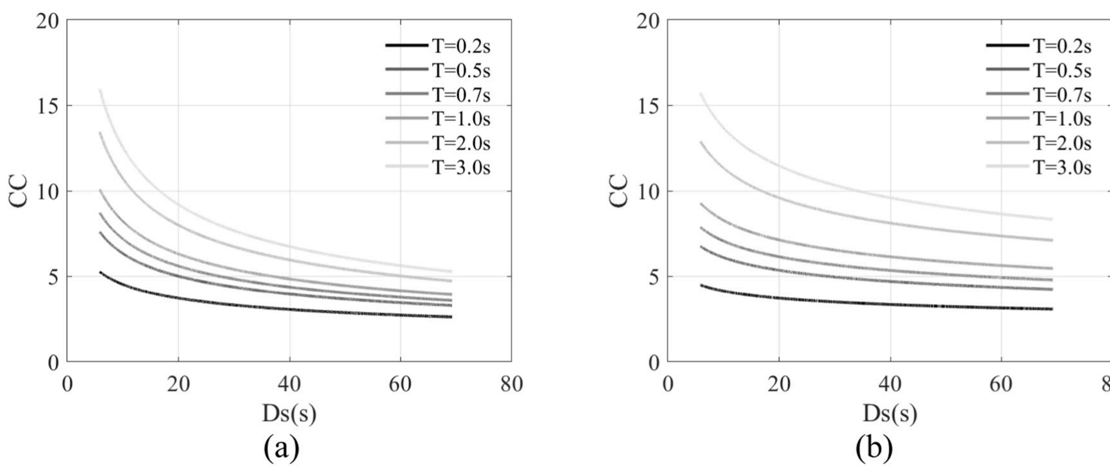

Fig. 10. Median predicted collapse capacity against duration for systems with varying period, θ-α = 0.02, μ_c= 1.0 for: (a) bilinear hysteresis, and (b) pinching hysteresis.

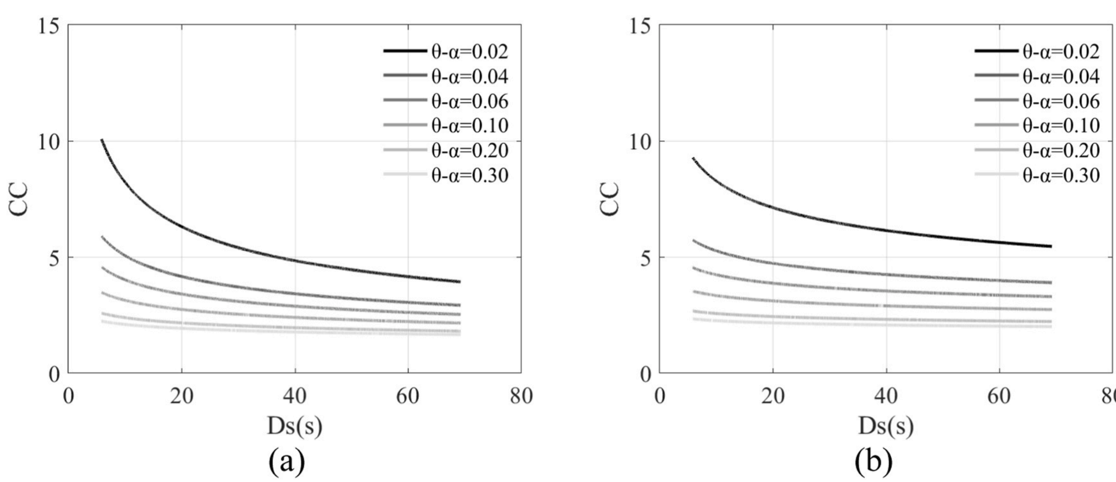

Fig. 11. Median predicted collapse capacity against duration for systems with T = 1.0 s, varying θ-α, μ_c= 1.0 for: (a) bilinear hysteresis, and (b) pinching hysteresis.

[19,22].

5. Comparative assessments

In order to highlight the merits of the regression model, developed and described in the previous section, it is compared herein to available

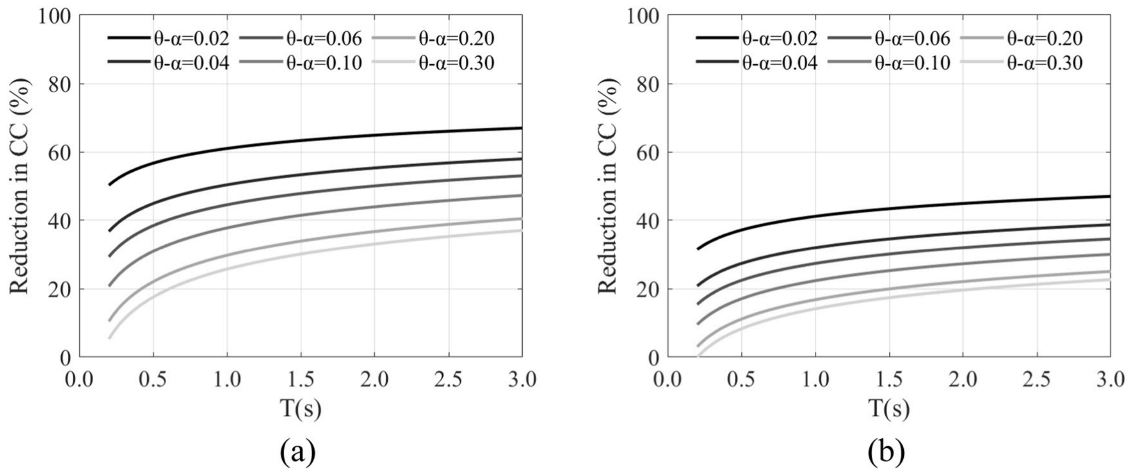

Fig. 12. Maximum percentage reduction in median collapse capacity against period for systems with varying P-Δ level for: (a) bilinear hysteresis, and (b) pinching hysteresis.

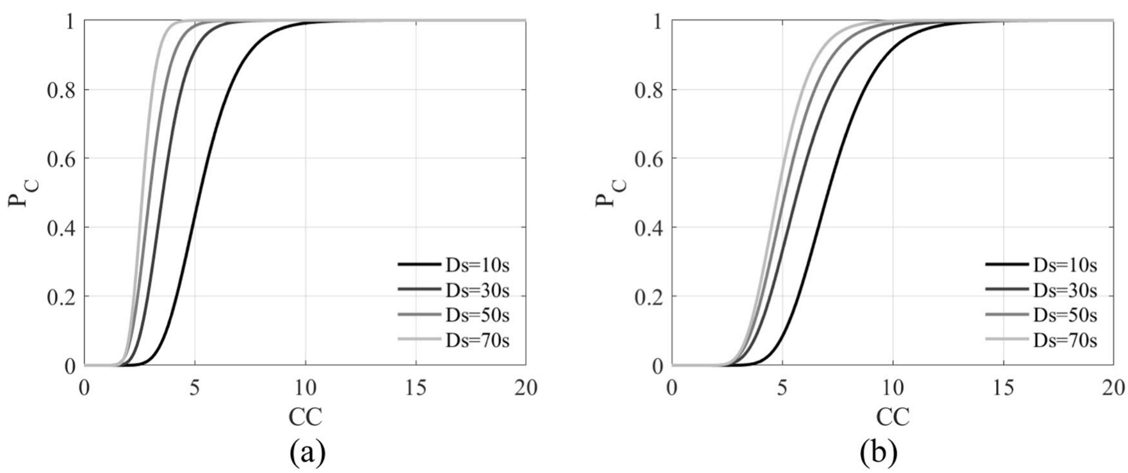

Fig. 13. Collapse fragility curves for systems with T = 3.0 s, θ-α = 0.04, μ_c= 6.0 for: (a) bilinear hysteresis, and (b) pinching hysteresis.

predictive relationships in the literature. It should be noted that most available collapse capacity models are derived using only short-duration records, thus completely disregarding the duration effect. Therefore, such duration-independent models are not considered in the comparisons presented herein.

5.1. Duration-based models

Three of the most relevant collapse capacity models that incorporate the strong motion duration are summarised in Table 7. All these include the fundamental period T_1, while the rest of the predictors and the response variables, as well as the methodology employed, vary.

The models proposed by Bernal [20] and Raghunandan and Liel [14] are based on substantially different assumptions to the method employed herein. The former does not account for the response spectra differences of the records used in its development, thus introducing bias in the results, while the latter considers the spectral shape effect implicity, by adopting the inelastic spectral displacement $S_{\{di\}}$ as the intensity measure. Therefore, these two predictive relationships are not comparable to those proposed herein. In [35], the effects of spectral shape were included by using the parameter SaRatio as a predictor of the spectral acceleration at collapse. Based on IDAs of 51 reinforced concrete ductile moment frames, subjected to a set of 88 records, Eqs. (12)–(14) were derived.

$$\ln S_{ac} = c_0 + c_{dur} \bullet \ln Ds + c_{ss} \bullet \ln SaRatio \tag{12}$$

$$c_{ss} = 0.99 - 0.13 \ln T_1 \tag{13}$$

$$c_{dur} = -0.21 + 0.058 \ln T_1 \tag{14}$$

In contrast, the parameter SaRatio is not considered in the regression analyses carried out in the present work, as the spectral shape is controlled by selecting spectrally matched records to the target Eurocode 8 spectrum. Thus, to enable comparisons between the two studies, a regression model based on Eq. 12 can be refitted to the IDA results. The

Table 7
Duration-based collapse capacity models.

Model	Response variable	Independent variables
Bernal [20]	S_a	$Ds_{5\text{-}95}$, T_1, θ, PGV, PGD
Raghunandan and Liel [14]	$S_{\{di\}}$	$Ds_{5\text{-}95}$, T_1, B_F
Chandramohan et al. [35]	S_a	$Ds_{5\text{-}95}$, T_1, SaRatio

Table 8
Regression coefficients for bilinear and pinching hysteresis.

	m	n	k
Bilinear	1.4141	-0.2295	0.7285
Pinching	1.1532	-0.1195	1.0903

relevant functional form is given by Eq. 15 and the regression coefficients are provided in Table 8.

$$\ln CC = k_0 + k_{dur} \bullet \ln Ds + k_{ss} \bullet \ln SaRatio \quad (15)$$

By inspecting the residuals of this regression model, the structural properties that should be included in the predictors can be identified. Plots of the standardised residuals against the period, P-Δ level, and ductility are given in Fig. 14 for bilinear hysteresis, while similar results can be obtained for pinching systems. Linear lines of best fit and LOESS fit lines (locally weighted smoothing) are also shown, indicating that the residuals depend on the period and P-Δ level to a great extent, while a smaller dependence on the ductility can also be discerned. Hence, it is crucial to include the period, the P-Δ effect, and possibly the ductility among the predictors, as undertaken herein. Estimating the regression coefficients as a fuction of the period only is expected to result in less accurate predictions.

5.2. Models based on short and long record sets

Due to the limited number of continuous duration-based collapse capacity models, the predictive relationships proposed in this paper are also compared to discrete duration models, which predict the median collapse capacity for groups of short or long duration records. The underlying differences between such models and those developed herein lie in the method of incorporating the duration. In the former case, sets of spectrally equivalent long and short records are assembled and collapse capacity models for each duration group are developed. In contrast, in this investigation, duration is included in the regression models, thus allowing prediction of the capacity based on specific target duration levels rather than using a broad characterisation of long and short ground motions.

Although many studies have examined the duration effect by using spectrally equivalent records, only references [22] and [19] appear to have provided relevant predictive equations. The latter is employed herein, as it refers to ductile systems. The two models are compared in Fig. 15, considering bilinear and pinching systems with a period of 1.0 s, P-Δ level of 0.04, and ductility of 2.0. The IDA-based capacities at which the continuous model was fitted are also shown with circles. The median predicted capacities are in relatively good agreement at the long duration range (Ds>25 s), where the model developed in this study becomes flatter. On the other hand, larger deviations are observed between the two studies at short duration levels (Ds≤25 s), as the variation of collapse capacity with duration is not captured in the discrete model. The largest differences between the two methods occur at duration levels just below 25 s, due to the abrupt change in the discrete model, which overestimates the capacity by 39% for the bilinear and 24% for the pinching SDOF examined herein.

Median long- and short-duration collapse capacity spectra based on the two studies are compared in Fig. 16, assuming bilinear hysteresis and a fixed ductility level of 1.0. The median duration of the long and short record sets used in the discrete models are plugged into the present model, to obtain comparable results. It becomes clear that the collapse spectra are in close agreement, particularly for the long duration group. In the case of short records, the model developed herein tends to provide higher estimates of collapse capacity; however, a relatively good agreement is still maintained. Similar observations can be made for different levels of ductility and pinching hysteresis. Hence, although different ground motion records have been used, the median estimates of collapse capacity from the two models are similar, when appropriate duration values are employed in the relationships proposed in this paper.

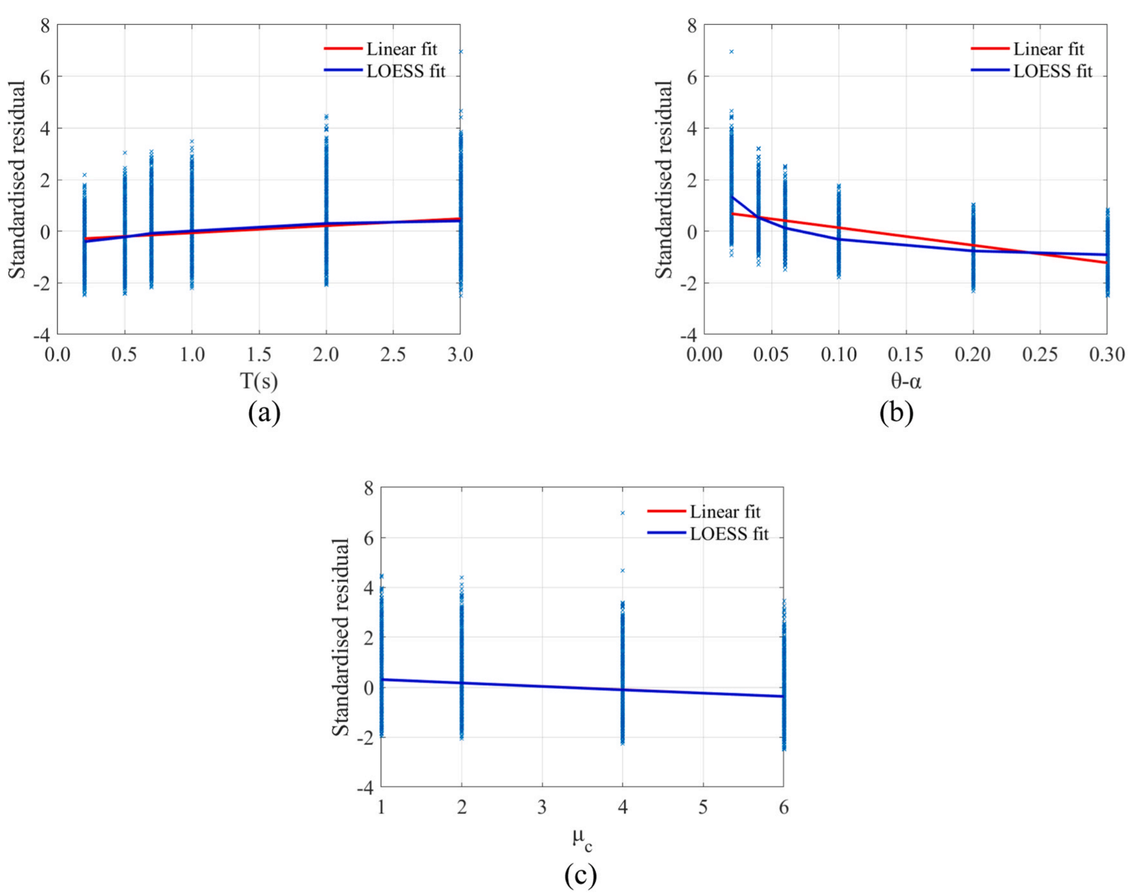

Fig. 14. Standardised residuals of the bilinear model against: (a) period, (b) level of P-Δ, and (c) ductility.

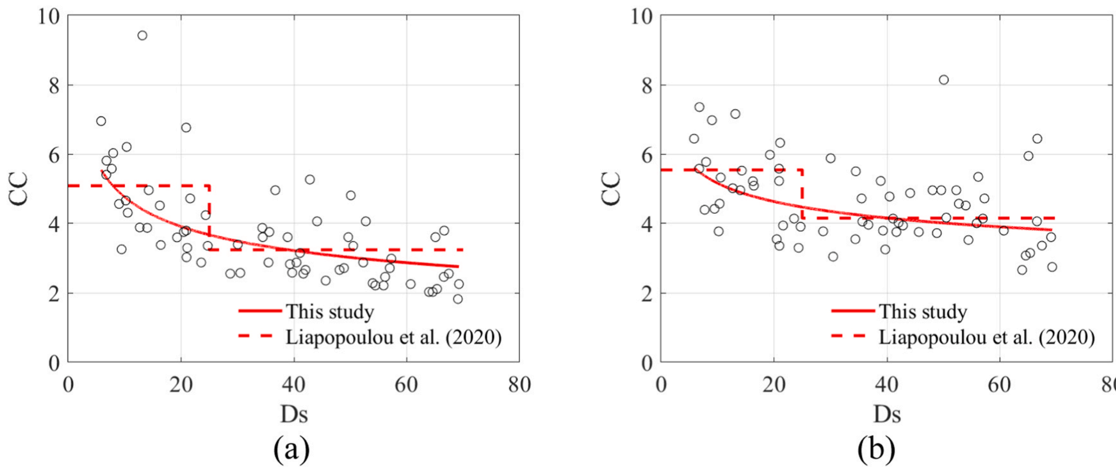

Fig. 15. Median predicted collapse capacity against duration from this study (solid lines) and from reference [19] (dashed lines) for systems with T = 1.0 s, θ-α = 0.04, μ_c= 2.0, and: (a) bilinear hysteresis, and (b) pinching hysteresis. Collapse capacities from this study are shown with circles.

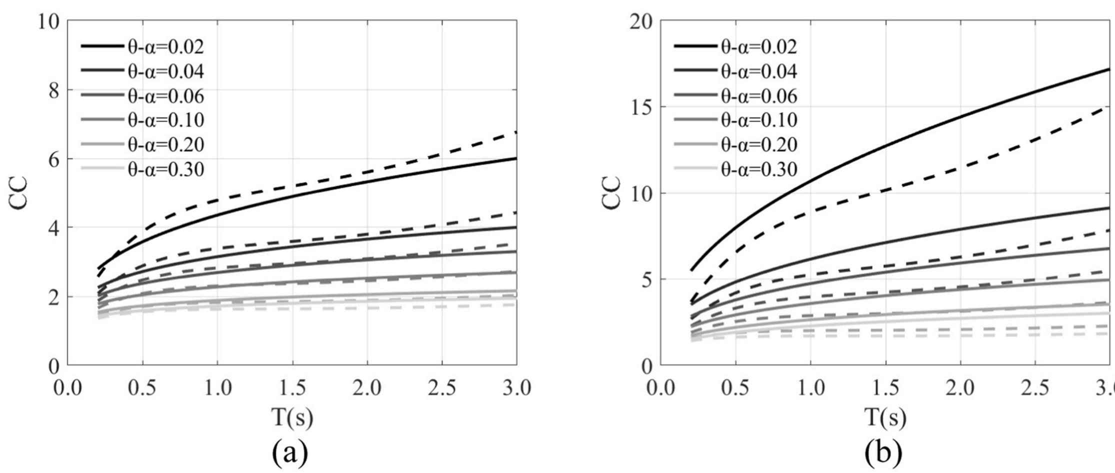

Fig. 16. Collapse capacity spectra from this study (solid lines) and from reference [19] (dashed lines) for systems with μ_c= 1.0, bilinear hysteresis, and: (a) long duration, and (b) short duration.

6. Conclusions

In this paper, a novel collapse capacity prediction model has been developed, based on IDA results of bilinear and pinching SDOF systems. Apart from characteristic properties of the structural models, the ground motion duration, quantified by means of the 5–75% significant duration, was also included in the predictors. The period, P-Δ level, and ductility of the SDOFs were varied in the ranges of 0.2 s–3.0 s, 0.02–0.30, and 1.0–6.0, respectively. The records used in the analyses exhibited up to 70 s strong motion duration and were appropriately scaled to match the same Eurocode 8-based response spectrum. In total, 67 records from the NGA-West-2, the Kik-net, and K-Net databases were selected.

Based on correlation analyses, the 5–75% significant duration was found to be more strongly related to collapse capacity than other ground motion parameters examined, namely the Arias Intensity and Husid plot slope, and was therefore regarded as the most appropriate predictor of collapse. Among the structural properties considered in this research (period, P-Δ level, and ductility), all three exhibited high correlation coefficients with collapse capacity. The period and P-Δ level also showed relatively large best-fit line slopes, indicating their importance as collapse predictors. After developing appropriate functional forms for the mean and the variance, iteratively reweighted least squares regression analyses were carried out to fit the collapse capacity data for each hysteresis type.

Employing the derived models, the collapse capacity was shown to decline as duration increases, with the rate of this reduction depending on the period, P-Δ level, and hysteresis, as well as the duration itself. At shorter durations, higher reduction rates were noted, compared to longer duration levels. The maximum duration-induced capacity reduction was about 67%, considering the extreme duration values of the selected records, and was observed for a bilinear SDOF with 3.0 s period and 0.02 P-Δ level. This indicates that if short records are exclusively employed in sites where long ground motions are also anticipated, the collapse capacity may be significantly overestimated.

To demonstrate the value of the proposed regression models, these were compared to similar models available in the literature, indicating the need to include not only the period but also the P-Δ level and the ductility, as undertaken in the present study. In addition, the proposed expressions were shown to advance current discrete duration models, which provide constant capacity estimates for short and long duration, thus lacking the ability to predict the capacity for a given target duration. Such models may overestimate the capacity at duration values close to the threshold between short and long duration. Nevertheless, the median long and short collapse capacity spectra derived with the two methods were in good agreement, provided that consistent duration levels are considered.

Overall, the expressions proposed in this paper enable collapse capacity predictions directly based on the expected strong motion duration. This offers a simple, yet reliable, method for integrating duration in collapse assessment procedures at the early stages of the design, which is not explicitly addressed in current seismic design standards. Given the limited number of duration-based capacity prediction models, the expressions derived herein contribute to the improvement of simplified capacity assessment procedures. It should be noted, however, that their applicability is limited by the range of structural properties and duration values based on which they were developed, as well as the spectral shape of the selected records. The effects of different target response spectra or special ground motion characteristics, such as the presence of pulses, may require further assessment in future studies. It is also worth noting that this study is a first fundamental step in ongoing work by the authors [36] on the role of duration in real frames. As part of this, the relationship between the influence of duration in SDOF and MDOF models has been examined, indicating that the trends presented herein based on SDOF results are also applicable to MDOF models. However, to predict accurately the response at the frame level, the SDOF-based collapse capacities need to be calibrated for the specific frame characteristics.

CRediT authorship contribution statement

Maria Liapopoulou: Conceptualization, Methodology, Software, Validation, Formal analysis, Investigation, Resources, Data Curation, Writing - Original Draft, Visualization. **Peter J. Stafford:** Conceptualization, Methodology, Resources, Writing - Review & Editing, Supervision. **Ahmed Y. Elghazouli:** Conceptualization, Methodology, Resources, Funding Acquisition, Writing - Review & Editing, Supervision, Project administration.

Declaration of Competing Interest

The authors declare that they have no known competing financial interests or personal relationships that could have appeared to influence the work reported in this paper.

Data availability

Data will be made available on request.

Acknowledgments

The first author would like to acknowledge the support provided by the Skempton Scholarship from Imperial College London and by the scholarship from Onassis Foundation in Greece.

Appendices.

Record processing

The records from the Japanese database (K-Net and kik-net), which were initially provided as raw data, were subjected to processing, according to recommendations from previous studies. The basic steps of this procedure are summarised herein. Firstly, baseline correction was implemented following the procedure in [37]. Next, the noise window was defined according to the method in [38], which picks the noise interval based on duration and mean energy criteria. The Fourier amplitude spectra of the signal and the noise window were then smoothened using the Konno-Ohmachi filter with b= 40 [39], and the signal-to-noise ratio (SNR) spectrum was computed. The cut-off frequencies were then selected according to the recommendations in [40], with the low-cut frequency, f_{lc}, corresponding to a SNR of 3, and the high-cut frequency, f_{hc}, to a SNR of 2. If the high-cut frequency was equal or greater than the Nyquist frequency, then no high-cut filtering was applied, as this would result in no difference [41]. Before filtering the record, by means of a 4th order acausal Butterworth filter with the selected cut-off frequencies, a cosine taper was applied at the first and last 5% of the baseline corrected signal and the acceleration time history was zero-padded with an appropriate length of pads, as suggested in [41]. Finally, the processed records were checked to ensure that their usable frequency bandwidth, which spans from 1.25 f_{lc} to 0.8 f_{hc} [42], included the range of frequencies of the SDOF systems examined in this study. The displacement and velocity end values, as well as their decay slopes towards the end, were also checked, using the criteria postulated in [37]. Records that did not satisfy these requirements were not included in the database.

Prediction model diagnostics

This section presents some additional diagnostic plots of the regression models derived in this paper. Figure B.1 shows the m and n coefficients estimated from OLS linear regression (Eq. 4), as well as the corresponding values predicted from Eqs. 5 and 6, for pinching systems. Similar to the case of bilinear hysteresis (Fig. 8), the agreement between the equations and the regression estimates is remarkable for the m values, and relatively good for the n values, in most cases.

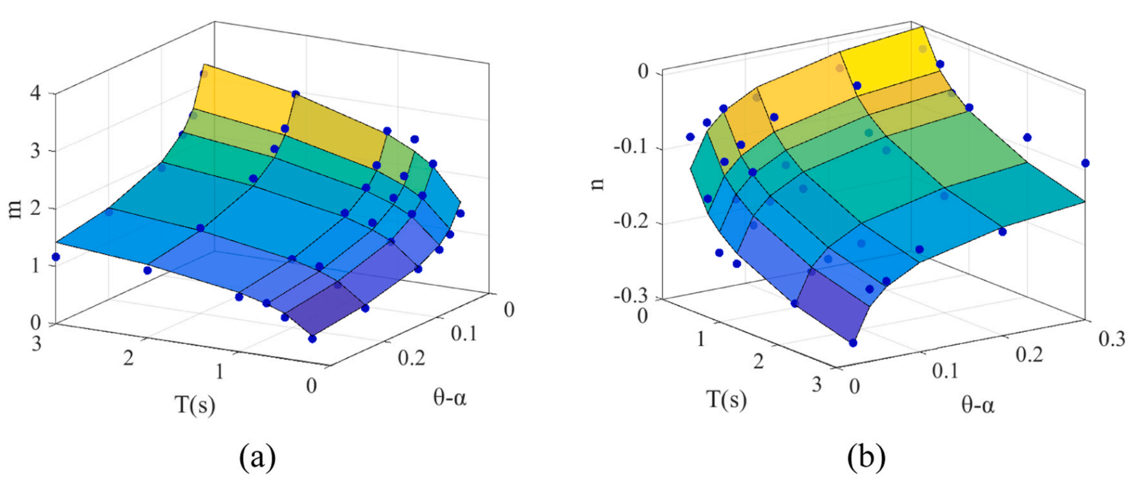

Fig. B1. Predicted (surface plot) and target (spheres) coefficients m and n for pinching systems with μ_c= 1.0.

.

Plots of the standardised residuals against the fitted values for the developed bilinear and pinching models are illustrated in Figure B.2. Linear trend lines are also shown with red colour. The residuals distribution is relatively uniform over the range of the response, without exhibiting any specific pattern, as indicated also by the horizontal trend lines. Consequently, the standardised residuals can be considered homoscedastic.

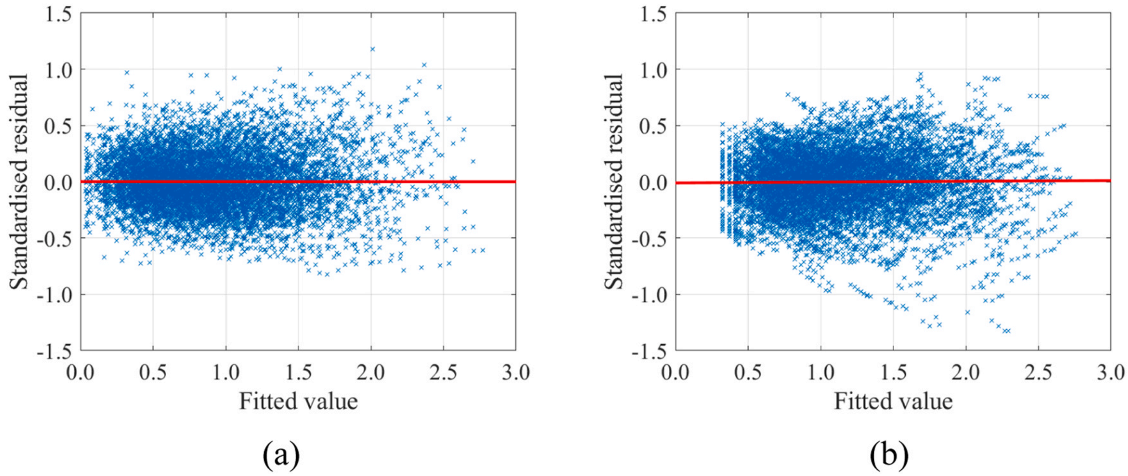

Fig. B2. Standardised residuals against fitted values for: (a) bilinear model, and (b) pinching model.

.

References

[1] CEN. European Standard EN 1998-3:2005 Eurocode 8: Design of structures for earthquake resistance—Part 3: Assessment and retrofitting of buildings. Brussels: European Committee for Standardization; 2005.

[2] FEMA. Quantification of building seismic performance factors. Washington, D.C.: U.S. Dept. of Homeland Security, FEMA; 2009.

[3] Vamvatsikos D, Cornell CA. Incremental dynamic analysis. Earthq Eng Struct Dyn 2002;31(3):491–514. https://doi.org/10.1002/eqe.141.

[4] Miranda E, Akkar SD. Dynamic instability of simple structural systems. J Struct Eng 2003;129(12):1722–6. https://doi.org/10.1061/(ASCE)0733-9445(2003)129:12(1722).

[5] Adam C, Jäger C. Seismic collapse capacity of basic inelastic structures vulnerable to the P-delta effect. Earthq Eng Struct Dyn 2012;41(4):775–93. https://doi.org/10.1002/eqe.1157.

[6] Vamvatsikos D, Akkar S.D, Miranda E. 2009. Strength reduction factors for the dynamic instability of oscillators with non-trivial backbones. Conference on computational methods in structural dynamics and earthquake engineering. Rhodes.Vamvatsikos D., Akkar S.D., Miranda E. Strength reduction factors for the dynamic instability of oscillators with non-trivial backbones. Computational methods in structural dynamics and earthquake engineering. Rhodes; 2009.

[7] Han SW, Moon K, Chopra AK. Application of MPA to estimate probability of collapse of structures. Earthq Eng Struct Dyn 2010;39(11):1259–78. https://doi.org/10.1002/eqe.992.

[8] Krawinkler H, Zareian F. Prediction of collapse—how realistic and practical is it, and what can we learn from it? Struct Des Tall Spec Build 2007;16(5):633–53. https://doi.org/10.1002/tal.433.

[9] Shafei B, Zareian F, Lignos DG. A simplified method for collapse capacity assessment of moment-resisting frame and shear wall structural systems. Eng Struct 2011;33(4):1107–16. https://doi.org/10.1016/j.engstruct.2010.12.028.

[10] Akai TJ. Applied Numerical Methods for Engineers. Toronto: Wiley; 1994.

[11] Fairhurst M, Bebamzadeh A, Ventura CE. Effect of ground motion duration on reinforced concrete shear wall buildings. Earthq Spectra 2019;35(1):311–31. https://doi.org/10.1193/101117EQS201M.

[12] Bravo-Haro MA, Elghazouli AY. Influence of earthquake duration on the response of steel moment frames. Soil Dyn Earthq Eng 2018;115:634–51. https://doi.org/10.1016/j.soildyn.2018.08.027.

[13] Chandramohan R, Baker JW, Deierlein GG. Quantifying the influence of ground motion duration on structural collapse capacity using spectrally equivalent records. Earthq Spectra 2016;32(2):927–50. https://doi.org/10.1193/122813EQS298MR2.

[14] Raghunandan M, Liel AB. Effect of ground motion duration on earthquake-induced structural collapse. Struct Saf 2013;41:119–33. https://doi.org/10.1016/j.strusafe.2012.12.002.

[15] Raghunandan M, Liel AB, Luco N. Collapse risk of buildings in the Pacific northwest region due to subduction earthquakes. Earthq Spectra 2015;31(4):2087–115. https://doi.org/10.1193/012114EQS011M.

[16] Husid RL. Características de terremotos. Análisis general. Rev IDIEM 1969;8(1):21–42.

[17] Bertero VV, Mahin SA, Herrera RA. Aseismic design implications of near-fault san fernando earthquake records. Earthq Eng Struct Dyn 1978;6(1):31–42. https://doi.org/10.1002/eqe.4290060105.

[18] Zengin E, Abrahamson NA, Kunnath S. Isolating the effect of ground-motion duration on structural damage and collapse of steel frame buildings. Earthq Spectra 2020;36(2):718–40. https://doi.org/10.1177/8755293019891720.

[19] Liapopoulou M, Bravo-Haro MA, Elghazouli AY. The role of ground motion duration and pulse effects in the collapse of ductile systems. Earthq Eng Struct Dyn 2020;49(11):1051–71. https://doi.org/10.1002/eqe.3278.

[20] Bernal D. Instability of buildings subjected to earthquakes. J Struct Eng 1992;118(8):2239–60. https://doi.org/10.1061/(asce)0733-9445(1992)118:8(2239).

[21] Trifunac MD, Brady AG. A study on the duration of strong earthquake ground motion. Bull Seismol Soc Am 1975;65(3):581–626. https://doi.org/10.1061/(asce)0733-9399(1990)116:6(1426).

[22] Bravo-Haro MA, Liapopoulou M, Elghazouli AY. Seismic collapse capacity assessment of SDOF systems incorporating duration and instability effects. Bull Earthq Eng 2020;18(7):3025–56. https://doi.org/10.1007/s10518-020-00829-9.

[23] Adam C, Jäger C. Simplified collapse capacity assessment of earthquake excited regular frame structures vulnerable to P-delta. Eng Struct 2012;44:159–73. https://doi.org/10.1016/j.engstruct.2012.05.036.

[24] McKenna F. OpenSees: a framework for earthquake engineering simulation. Comput Sci Eng 2011;13(4):58–66.

[25] Ancheta TD, Darragh RB, Stewart JP, Seyhan E, Silva WJ, Chiou BSJ, et al. NGA-West2 database. Earthq Spectra 2014;30(3):989–1005. https://doi.org/10.1193/070913EQS197M.

[26] Kinoshita S. Kyoshin Net (K-NET). Seismol Res Lett 1998;69(4):309–32.

[27] Aoi S. New Japanese uphole/downhole strong-motion observation network: KiK-net. Seismol Res Lett 2000;72:239.

[28] Shahi SK, Baker JW. An efficient algorithm to identify strong-velocity pulses in multicomponent ground motions. Bull Seismol Soc Am 2014;104(5):2456–66. https://doi.org/10.1785/0120130191.

[29] CEN. European Standard EN 1998-1:2004 Eurocode 8: Design of structures for earthquake resistance—Part 1: General rules, seismic actions and rules for buildings. Brussels: European Committee for Standardization; 2004.

[30] Somerville PG, Smith NF, Graves RW, Abrahamson NA. Modification of empirical strong ground motion attenuation relations to include the amplitude and duration effects of rupture directivity. Seismol Res Lett 1997;68(1):199–222.

[31] Foschaar J.C., Baker J.W., Deierlein G.G. 2012. Preliminary assessment of ground motion duration effects on structural collapse. 15th world conference on earthquake engineering. Lisboa.

[32] Vamvatsikos D, Cornell CA. Direct estimation of the seismic demand and capacity of oscillators with multi-linear static pushovers through IDA. Earthq Eng Struct Dyn 2006;35(9):1097–117. https://doi.org/10.1002/eqe.573.

[33] Arias A. Measure of Earthquake Intensity. Santiago De Chile: Massachusetts Inst. of Tech., Cambridge. Univ. of Chile; 1970.

[34] Ibarra LF, Krawinkler H. Global Collapse of Frame Structures under Seismic Excitations. John A Blume Earthquake Engineering Center; 2005.

[35] Chandramohan R, Baker J.W, Deierlein G.G., 2018. Accounting for the influence of ground motion response spectral shape and duration in the equivalent lateral force design procedure. 11th U.S. national conference on earthquake engineering. Los Angeles.
[36] Liapopoulou M. Ultimate seismic response of steel framed structures. PhD thesis. Imperial College London; 2018.
[37] Dawood HM, Rodriguez-Marek A, Bayless J, Goulet C, Thompson E. A flatfile for the KiK-net database processed using an automated protocol. Earthq Spectra 2016; 32(2):1281–302. https://doi.org/10.1193/071214eqs106.
[38] Perron V, Laurendeau A, Hollender F, Bard P, Gélis Céline, Traversa P, et al. Selecting time windows of seismic phases and noise for engineering seismology applications: a versatile methodology and algorithm. Bull Eathquake Eng 2018;16 (6):2211–25. https://doi.org/10.1007/s10518-017-0131-9.
[39] Konno K, Ohmachi T. Ground-motion characteristics estimated from spectral ratio between horizontal and vertical components of microtremor. Bull Seismol Soc Am 1998;88(1):228–41. https://doi.org/10.1785/BSSA0880010228.
[40] Bahrampouri M, Rodriguez-Marek A, Shahi S, Dawood H. An updated database for ground motion parameters for KiK-net records. Earthq Spectra 2021;37(1):505–22. https://doi.org/10.1177/8755293020952447.
[41] Boore DM, Bommer JJ. Processing of strong-motion accelerograms: needs, options and consequences. Soil Dyn Earthq Eng (1984) 2005;25(2):93–115. https://doi.org/10.1016/j.soildyn.2004.10.007.
[42] Bayless J, Abrahamson NA. Summary of the BA18 ground-motion model for fourier amplitude spectra for crustal earthquakes in California. Bull Seismol Soc Am 2019; 109(5):2088–105. https://doi.org/10.1785/0120190077.